Variations in the Modal Characteristics of A Telescopically Deploying Beam

Anthony K. Amos†
Penn State University
University Park, PA 16802

SUMMARY

The equations of motion for a two-segment deploying telescopic beam are derived through application of Lagrange's equation. The outer tube of the beam is fixed at one end and the inner tube slides freely relative to the fixed segment. The resulting nonlinear, non-autonomous set of equations is linearized and simplified to the standard Euler-Bernoulli partial differential equations for an elastic beam by freezing the deployment process at various stages of deployment, and examining the small amplitude and natural modes of vibration of the resulting configuration. Application of the natural boundary conditions and compatibility of motion relations for the two segments in their common region of overlap leads to a transcendental characteristic equation in the frequency parameter βL, where

$$(\beta L)^4 = \frac{\omega^2 m L^4}{EI};$$

L = length of beam

m = mass / unit length of fixed beam segment

EI = flexural rigidity of the beam

ω = frequency

Numerical solution of the equation for the characteristic roots determines the modal frequencies, and the corresponding mode shapes are obtained from the general solution of the Euler-Bernoulli equation tailored to the natural boundary conditions.

Sample results of modal frequencies and shapes are presented for various stages of deployment and discussed. It is shown that for all intermediate stages of deployment (between 0% and 100%) the spectral distribution is drastically altered by the appearance of regions of very closely spaced modal frequencies. The sources of this modal agglomeration are explored.

---

† *Professor of Aerospace Engineering*

INTRODUCTION

The dynamics of spacecraft in earth orbit or interplanetary travel is uniquely different from earth-bound system dynamics in as much as equilibrium and stability result from the strong interactions among the laws of rigid body dynamics and those of flexible vibrational motions. If in addition, the spacecraft undergoes spatial and temporal redistribution of inertial and stiffness properties as during deployment and assembly operations, the dynamics of this configuration evolution must also be accommodated in this self-contained dynamic system, without uncontrollable deviations from desired flight paths and attitude configurations.

The material presented in this paper is part of an ongoing basic research effort to develop greater understanding of and appreciation for these interactions, and in the process to develop analytical procedures for high fidelity simulations of on-orbit operations needed for the validation of designs of future systems prior to their construction on-orbit. Both of these research objectives have high relevance to future civilian and military space systems which are expected to be constructed on orbit. For many of the members used in the construction, critical design loads can be expected to occur from handling loads during construction.

One major thrust of the ongoing research is the modeling of selected deployment mechanisms isolated from their orbiting parent spacecraft, and the systematic investigation of their dynamic characteristics as influenced by design, configurational and deployment parameters. A two-segment telescoping beam is one such mechanism, and the subject of this paper.

Problem Definition

Determination of the natural modes of vibration of a deploying two-segment telescopic beam at various stages of deployment is the specific problem addressed in this paper. The conceptual physical model is that of a non-uniform beam comprised of an inner tube sliding freely inside an outer tube which is cantilevered from one end. Figure 1 illustrates the physical model, with the beam in a partially deployed configuration. Both tubes are considered to be thin-walled, and their diameters are sufficiently large compared to the wall thickness so that the two tubes can be considered to have the same flexural rigidity (I), area (A), and mass per unit length(m). The natural vibration frequencies and mode shapes of this model are to be determined for several stages of deployment between 0% and 100%.

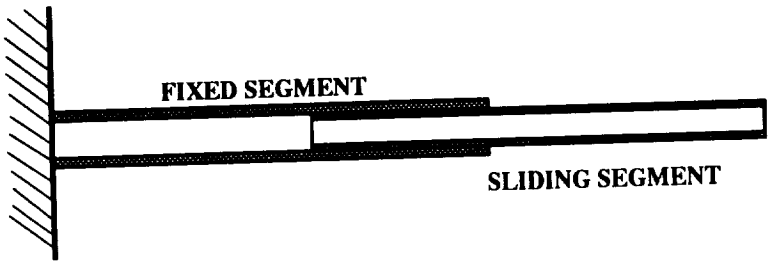

Figure 1: Telescopic Beam

MATHEMATICAL MODELING

Equations of Motion

The idealized model comprises two beams sliding freely relative to each other, as shown in Figure 2 below. The overlapping segments of the two are constrained to move together as a unit. The equations of motion are developed from application of Lagrange's equation which can be stated as:

$$\frac{d}{dt}\left(\frac{\partial T}{\partial \dot{q}_j}\right) - \frac{\partial T}{\partial q_j} + \frac{\partial V}{\partial q_j} = 0 \qquad (1)$$

where

T = Kinetic energy of the system

V = Potential energy of the system

$= U - W_e$

U = Strain Energy of the system

W_e = Virtual Work of external forces

q_j = Generalized coordinate

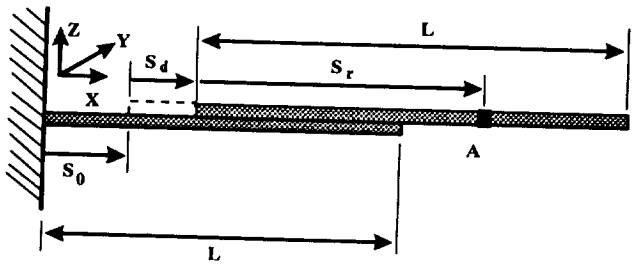

Figure 2: Idealized Telescopic Beam

Equations for the sliding segment:

With reference to the above figure, let

S_0 be the position of the overlap end of the sliding segment at some reference time t_0

S_d is the displacement of the end due to deployment motion

S_r is the deformed position of the reference point A

X_r is the Eulerian coordinate of A

v is the displacement of A in the y-direction

w is the displacement of A in the z-direction

Then

$$S_d = \int_{t_0}^{t} U_D dt \tag{2}$$

$$S_r = X_r + u_e - \frac{1}{2}\int_0^{X_r}\left[\left(\frac{\partial v}{\partial x}\right)^2 + \left(\frac{\partial w}{\partial x}\right)^2\right]dx \tag{3}$$

where

U_D = Deployment velocity

u_e = Displacement of A due to elasticity

The velocity vector of A is then given by:

$$\dot{\underline{r}}_A \cong \left[U_D + \dot{u}_e - \frac{1}{2}\left(\dot{v}\frac{\partial v}{\partial x} + v\frac{\partial \dot{v}}{\partial x} + \dot{w}\frac{\partial w}{\partial x} + w\frac{\partial \dot{w}}{\partial x}\right)\right]\hat{\underline{i}} + \dot{v}\hat{\underline{j}} + \dot{w}\hat{\underline{k}} \tag{4}$$

Now define a displacement u such that

$$\dot{u} = U_D + \dot{u}_e - \frac{1}{2}\left(\dot{v}\frac{\partial v}{\partial x} + v\frac{\partial \dot{v}}{\partial x} + \dot{w}\frac{\partial w}{\partial x} + w\frac{\partial \dot{w}}{\partial x}\right) \tag{5}$$

Then

$$\dot{\underline{r}}_A = \dot{u}\hat{\underline{i}} + \dot{v}\hat{\underline{j}} + \dot{w}\hat{\underline{k}} \tag{6}$$

The kinetic energy of the system can now be determined as

$$\begin{aligned} T &= \frac{1}{2}m\int_0^L \dot{\underline{r}}_A \bullet \dot{\underline{r}}_A dx \\ &= \frac{1}{2}m\int_0^L \left(\dot{u}^2 + \dot{v}^2 + \dot{w}^2\right)dx \end{aligned} \tag{7}$$

The strain energy and virtual work quantities can be expressed as

$$U = \frac{1}{2}\int_0^L \left[EI_y\left(\frac{\partial^2 v}{\partial x^2}\right)^2 + EI_z\left(\frac{\partial^2 w}{\partial x^2}\right)^2 + EA\left(\frac{\partial u_e}{\partial x}\right)^2\right]dx \tag{8}$$

$W_e = \int_0^L \left(p_y v + p_z w\right)dx$: where p_y and p_z are external distributed loads. (9)

It should be noted that in the above equations, the variable u introduced by definition is not a state variable like v and w, but is rather a function of the last two and the elastic displacement u_e. Hence the generalized coordinates are u_e, v, and w.

Performing the variations indicated in the Lagrange's equations, and noting that, as in Hamilton's Principle, admissible variations all vanish at the boundaries of the integration domain, the following nonlinear and non-autonomous equations result.

$$m\ddot{u} - EA\frac{\partial^2 u_e}{\partial x^2} = 0 \tag{10}$$

$$m\left[\ddot{v} - \frac{1}{2}\left(\ddot{u}\frac{\partial v}{\partial x} + \dot{u}\frac{\partial \dot{v}}{\partial x} + \dot{v}\frac{\partial \dot{u}}{\partial x}\right)\right] + EI_y\frac{\partial^4 v}{\partial x^4} = p_y \tag{11}$$

$$m\left[\ddot{w} - \frac{1}{2}\left(\ddot{u}\frac{\partial w}{\partial x} + \dot{u}\frac{\partial \dot{w}}{\partial x} + \dot{w}\frac{\partial \dot{u}}{\partial x}\right)\right] + EI_z\frac{\partial^4 w}{\partial x^4} = p_z \tag{12}$$

Equations for the Fixed Segment:

The above equations are directly applicable to the fixed segments with the modification that the quantity u is defined without the deployment velocity U_D, i.e.

$$\dot{u} = \dot{u}_e - \frac{1}{2}\left(\dot{v}\frac{\partial v}{\partial x} + v\frac{\partial \dot{v}}{\partial x} + \dot{w}\frac{\partial w}{\partial x} + w\frac{\partial \dot{w}}{\partial x}\right) \tag{13}$$

Characteristic Equations

For the purpose of determining the modal characteristics, the above equations of motion are reduced to a quasi-static form by dropping the deployment velocity related terms and all nonlinear terms to yield

$$m\ddot{u} - EA\frac{\partial^2 u_e}{\partial x^2} = 0 \tag{14A}$$

$$m\ddot{v} + EI\frac{\partial^4 v}{\partial x^4} = 0 \tag{14B}$$

$$m\ddot{w} + EI\frac{\partial^4 w}{\partial x^4} = 0 \tag{14C}$$

The equations are completely uncoupled and can be studied independently of one another. The following treatment is therefore confined to vibrations in the x-z plane, governed by the last of the three equations above. This is a standard beam equation of the Euler-Bernoulli type. The homogeneous part defines the modal characteristics of the beam system.

The general solution of the homogeneous equation is given by:

$$w(x,t) = (A_1 \cosh \beta x + A_2 \sinh \beta x + A_3 \cos \beta x + A_4 \sin \beta x)\sin(\omega t - \varphi) \qquad (15)$$
$$= \phi(x)\sin(\omega t - \varphi)$$

where

$$\beta^4 = \omega^2 \frac{m}{EI} \qquad (16)$$

At any stage of deployment, the telescopic beam can be idealized as a three segment beam as shown in Figure 3.

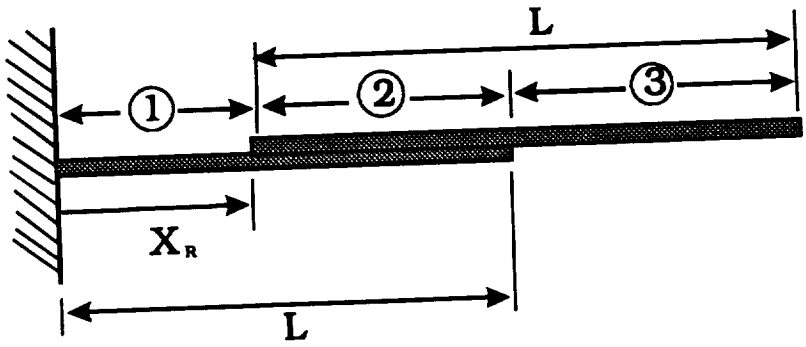

Figure 3: Uniform segments of the idealized telescopic beam.

The general solution above is applicable to each of the segments to yield

$$\phi(x) = \begin{Bmatrix} A_1 \cosh \beta_1 x + A_2 \sinh \beta_1 x + A_3 \cos \beta_1 x + A_4 \sin \beta_1 x; & 0 \le x \le X_R \\ B_1 \cosh \beta_2 x + B_2 \sinh \beta_2 x + B_3 \cos \beta_2 x + B_4 \sin \beta_2 x; & X_R \le x \le L \\ C_1 \cosh \beta_3 x + C_2 \sinh \beta_3 x + C_3 \cos \beta_3 x + C_4 \sin \beta_3 x; & L \le x \le L + X_R \end{Bmatrix} \qquad (17)$$

where

$$\beta_1^4 = \omega^2 \frac{m_1}{EI_1}; \quad \beta_2^4 = \omega^2 \frac{m_2}{EI_2}; \quad \beta_3^4 = \omega^2 \frac{m_3}{EI_3} \qquad (18)$$

m_1, m_2, m_3 are the mass per unit length of the respective segments;
EI_1, EI_2, and EI_3 are bending rigidities of the respective segments.

The constants in these displacement expressions are to be evaluated from a set of boundary conditions and compatibility relations at the two interfaces of the segments.

The boundary conditions are given by:

$$\begin{aligned}
&\phi_1(0) = 0 \\
&\frac{d\phi_1(0)}{dx} = 0 \\
&\frac{d^2\phi_3(L+X_R)}{dx^2} = 0 \\
&\frac{d^3\phi_3(L+X_R)}{dx^3} = 0
\end{aligned} \tag{19}$$

and the compatibility conditions are given by

$$\begin{aligned}
&\phi_1(X_R) = \phi_2(X_R) \\
&\frac{d\phi_1(X_R)}{dx} = \frac{d\phi_2(X_R)}{dx} \\
&EI_1\frac{d^2\phi_1(X_R)}{dx^2} = EI_2\frac{d^2\phi_2(X_R)}{dx^2} \\
&EI_1\frac{d^3\phi_1(X_R)}{dx^3} = EI_2\frac{d^3\phi_2(X_R)}{dx^3} \\
&\phi_2(L) = \phi_3(L) \\
&\frac{d\phi_2(L)}{dx} = \frac{d\phi_3(L)}{dx} \\
&EI_2\frac{d^2\phi_2(L)}{dx^2} = EI_3\frac{d^2\phi_3(L)}{dx^2} \\
&EI_2\frac{d^3\phi_2(L)}{dx^3} = EI_3\frac{d^3\phi_3(L)}{dx^3}
\end{aligned} \tag{20}$$

Introducing the appropriate functions into these conditions results in twelve homogeneous equations. The determinant of the coefficient matrix must vanish for non-trivial solution of the constants. Hence

$$\begin{vmatrix}
[A]_{2X4} & & \\
[B]_{4X4} & [C]_{4X4} & \\
 & [D]_{4X4} & [E]_{4X4} \\
 & & [F]_{2X4}
\end{vmatrix} = 0 \tag{21}$$

where

$$[A]=\begin{bmatrix}1 & 0 & 1 & 0\\ 0 & 1 & 0 & 1\end{bmatrix} \tag{22}$$

$$[B]=\begin{bmatrix}\cosh\alpha_1 & \sinh\alpha_1 & \cos\alpha_1 & \sin\alpha_1\\ \beta_1\sinh\alpha_1 & \beta_1\cosh\alpha_1 & -\beta_1\sin\alpha_1 & \beta_1\cos\alpha_1\\ EI_1\cosh\alpha_1 & EI_1\sinh\alpha_1 & -EI_1\cos\alpha_1 & -EI_1\sin\alpha_1\\ EI_1\sinh\alpha_1 & EI_1\cosh\alpha_1 & EI_1\sin\alpha_1 & -EI_1\cos\alpha_1\end{bmatrix} \tag{23}$$

$$[C]=\begin{bmatrix}-\cosh\alpha_2 & -\sinh\alpha_2 & -\cos\alpha_2 & -\sin\alpha_2\\ -\beta_2\sinh\alpha_2 & -\lambda_1\cosh\alpha_2 & \lambda_1\sin\alpha_2 & -\lambda_1\cos\alpha_2\\ -\lambda_1^2EI_2\cosh\alpha_2 & -\lambda_1^2EI_2\sinh\alpha_2 & \lambda_1^2EI_2\cos\alpha_2 & \lambda_1^2EI_2\sin\alpha_2\\ -\lambda_1^3EI_2\sinh\alpha_2 & -\lambda_1^3EI_2\cosh\alpha_2 & -\lambda_1^3EI_2\sin\alpha_2 & \lambda_1^3EI_2\cos\alpha_2\end{bmatrix} \tag{24}$$

$$[D]=\begin{bmatrix}\cosh\alpha_3 & \sinh\alpha_3 & \cos\alpha_3 & \sin\alpha_3\\ \sinh\alpha_3 & \cosh\alpha_3 & -\sin\alpha_3 & \cos\alpha_3\\ \cosh\alpha_3 & \sinh\alpha_3 & -\cos\alpha_3 & -\sin\alpha_3\\ \sinh\alpha_3 & \cosh\alpha_3 & \sin\alpha_3 & -\cos\alpha_3\end{bmatrix} \tag{25}$$

$$[E]=\begin{bmatrix}-\cosh\alpha_4 & -\sinh\alpha_4 & -\cos\alpha_4 & -\sin\alpha_4\\ -\lambda_2\sinh\alpha_4 & -\lambda_2\cosh\alpha_4 & \lambda_2\sin\alpha_4 & -\lambda_2\cos\alpha_4\\ -\lambda_2^2\cosh\alpha_4 & -\lambda_2^2\sinh\alpha_4 & \lambda_2^2\cos\alpha_4 & \lambda_2^2\sin\alpha_4\\ -\lambda_2^3\sinh\alpha_4 & -\lambda_2^3\cosh\alpha_4 & -\lambda_2^3\sin\alpha_4 & \lambda_2^3\cos\alpha_4\end{bmatrix} \tag{26}$$

$$[F]=\begin{bmatrix}\cosh\alpha_5 & \sinh\alpha_5 & -\cos\alpha_5 & -\sin\alpha_5\\ \sinh\alpha_5 & \cosh\alpha_5 & \sin\alpha_5 & -\cos\alpha_5\end{bmatrix} \tag{27}$$

and

$$\alpha_1=\beta_1X_R;\qquad \alpha_2=\beta_2X_R;\qquad \lambda_1=\frac{\beta_2}{\beta_1}$$

$$\alpha_3=\beta_2L;\qquad \alpha_4=\beta_3L;\qquad \lambda_2=\frac{\beta_3}{\beta_2}$$

$$\alpha_5=\beta_3(L+X_R) \tag{28}$$

The determinant equation is nondimensionalized by introducing

$$k=\beta_1L;\qquad \xi_R=\frac{X_R}{L} \tag{29}$$

Then

$$\alpha_1 = k\,\xi_R; \qquad \alpha_2 = \lambda_1 k\,\xi_R$$
$$\alpha_3 = \lambda_1 k; \qquad \alpha_4 = \lambda_1\,\lambda_2 k; \qquad \alpha_5 = \lambda_1\,\lambda_2 k(1+\xi_R) \tag{30}$$

SAMPLE RESULTS AND DISCUSSION

A numerical algorithm has been developed for solving the determinant equation for a specified number of the first consecutive eigenvalues (k_n) of the system and the corresponding eigenvectors representing the unknown coefficients of the displacement functions. The mode shapes are also calculated from the eigenvectors.

Table 1 lists the first 10 eigenvalues for a number of deployment stages. The first and last columns represent data for straight beams at the fully collapsed and at the fully deployed lengths. Figure 4 is a graphical display of the same data.

	βL for Different Deployment Stages(%)								
Mode #	0	5	10	25	50	75	90	95	100
1	1.8751	1.7739	1.6959	1.5325	1.3527	1.2115	1.1360	1.1120	0.9375
2	4.6941	4.4846	4.3572	4.0142	3.2388	2.6482	2.4442	2.3985	2.3470
3	7.8548	7.5461	7.3600	6.4243	5.0683	4.4664	4.1495	4.0468	3.9274
4	10.996	10.400	9.2000	8.5100	7.2910	6.2220	5.7000	5.5600	5.4980
5	14.137	10.503	9.2001	8.8400	7.3110	7.0904	6.7390	7.0318	7.0685
6	17.279	10.712	9.7300	9.0030	7.4015	7.1000	6.8010	7.1000	8.6395
7	20.420	10.812	9.8100	9.1010	7.5011	7.9100	7.3003	7.3103	10.210
8	23.562	10.910	9.9112	9.2004	7.6000	8.0100	7.6293	7.8314	11.781
9	26.704	11.000	10.010	9.6100	8.1545	8.1120	7.7002	8.0000	13.352
10	29.845	11.100	10.600	9.7200	8.2100	8.2004	7.9401	8.1506	14.922

Table 1: Frequency Parameter Variations with Deployment

Two trends are immediately evident from the data:

1. A compaction of the frequencies towards the lower end as deployment proceeds, thus increasing the modal density in regions of normal dynamic interest, and
2. The appearance of very close, nearly repeated roots from about the third mode upwards, for all the partially deployed configurations

The mode shapes provide clues as to the basis for these trends. Figures 5 through 10 show the first six mode shapes for the 0% and 5% deployment configurations. The first four mode shapes are very similar for the two configurations. The fifth and sixth differ markedly between the two configurations. The partially deployed configuration shows large motions in that portion of the deploying segment that protrudes from the fixed segment in comparison with the motions of the fixed segment. These modes can properly be described as " tip whip " modes, in analogy with the classical " antenna whip " motions of automobile radio antennas. The fixed segment is seen to be

vibrating essentially in its third mode under both the fifth and sixth coupled modes. It is clear that these two modes are the result of a coupling between the cantilevered modes of the fixed segment, and those of the protruding portion of the deploying segment. This coupling is believed to be the primary mechanism for the *agglomeration* of the modes.

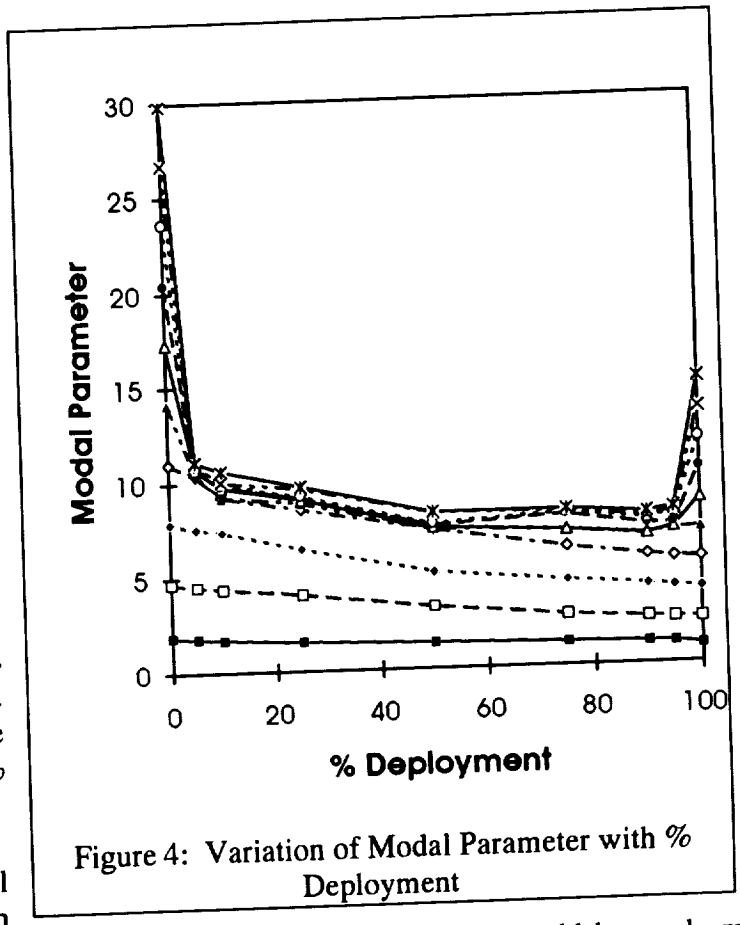

Figure 4: Variation of Modal Parameter with % Deployment

As the protruding portion of the deploying segment increases in length with deployment, its natural frequencies decrease and the coupling with fixed segment modes occurs at lower frequencies. Figures 11 through 13 illustrate the first five mode shapes at 25%, 50% and 90% deployment stages.

The observed changes in modal characteristics with deployment can be expected to have serious impacts. Control design for such a system would be made more difficult by virtue of the increased modal density and near coalescence of certain of the modes. Transient dynamic analyses cannot be readily performed by modal synthesis due to the continuous variations in the basis functions (mode shapes). Stability implications of the modal agglomeration can also be serious and will be explored in future studies.

CONCLUSION

The modal characteristics of the two-segment telescopic beam at all stages of partial deployment have been shown to vary drastically from those of either the completely collapsed or fully extended configurations. This variation manifests itself in an agglomeration of the modal frequencies near the lower end of the spectrum, and is attributable to the sharp discontinuities in mass and stiffness distributions between the region of overlap between the inner and outer segments and the non-overlap regions near the root and the free end respectively.

BIBLIOGRAPHY

1. Banerjee, A.K., and Kane, T.R., "Extrusion of a Beam from a Rotating Base," AIAA J. Guidance, vol 12, No 2, March-April 1989.

2. Kalaycioglu, S. and Misra, A.K., "Analytical Expressions for Vibratory Displacements of Deploying Appendages," AIAA paper 88-4250-CP, 1988.

3. Modi, V.J., and Ibrahim, A.M., "A General Formulation for Librational Dynamics of Spacecraft with Deploying Appendages," AIAA J. Guidance, vol 7, No 5, Sept-Oct 1984.

4. Tsuchiya, K., "Dynamics of a Spacecraft During Extension of Flexible Appendages," AIAA J. Guidance, vol 6, No 2, 1983.

5. Ibrahim, A.E., and Misra, A.K., "Attitude Dynamics of a Satellite During Deployment of Large Plate-Type Structures," AIAA J. Guidance, vol 5, No 5, Sep-Oct 1982.

6. Lips, K.W., and Modi, V.J., "Three-Dimensional Response Characteristics for Spacecraft with Deploying Flexible Appendages," AIAA J. Guidance and Control, vol 4, No 6, Nov-Dec 1981.

7. Tabarrok, B., Leech, C.M., and Kim, Y.I., " On the Dynamics of an Axially Moving Beam," J. Franklin Institute, vol 297, pp 201-220, 1974.

8. Atluri, S.N. and Amos, A.K.,(ed) Large Space Structures: Dynamics and Control, Springer-Verlag, 1988.

ACKNOWLEDGEMENT

This research is sponsored by the Air Force Office of Scientific Research (AFOSR) under Grant AFOSR-91-0155. The guidance and encouragement of the project director Dr. Spencer Wu are greatly appreciated.

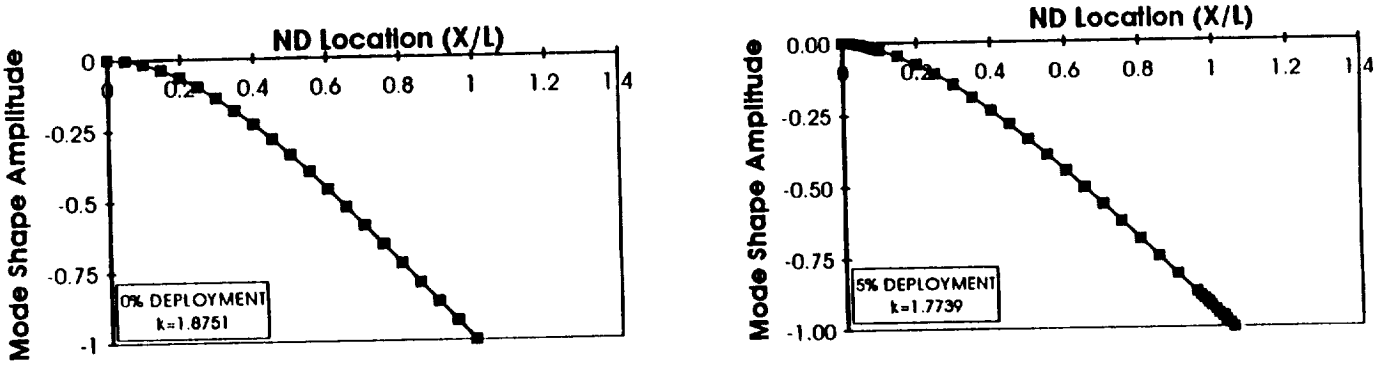

Figure 5: Mode 1 Shapes for 0% & 5% Deployment

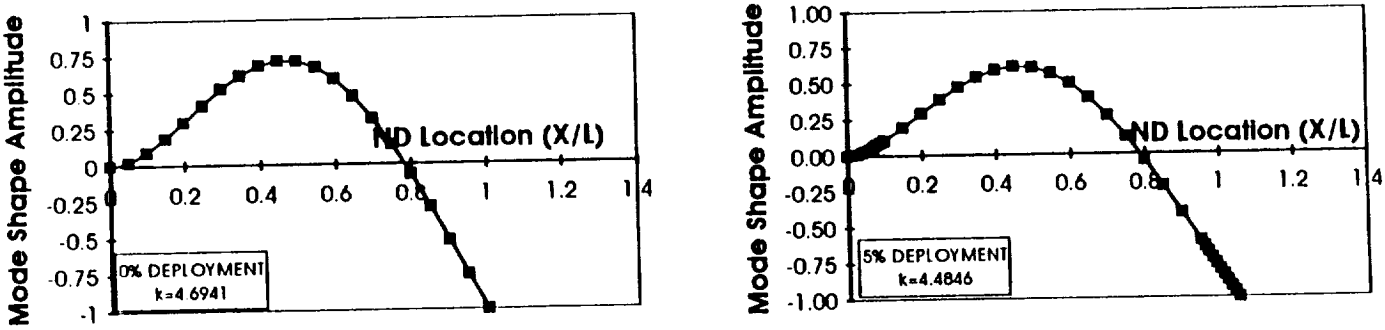

Figure 6: Mode 2 Shapes for 0% & 5% Deployment

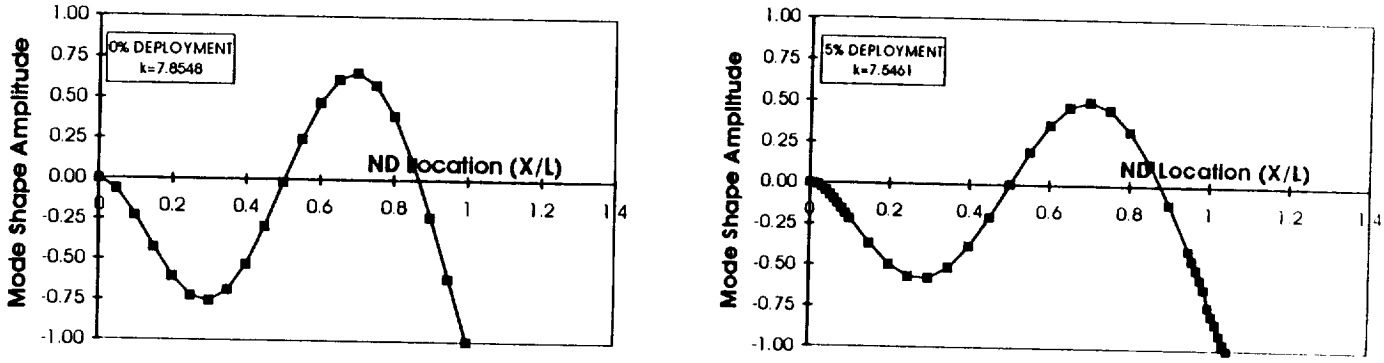

Figure 7: Mode 3 Shapes for 0% & 5% Deployment

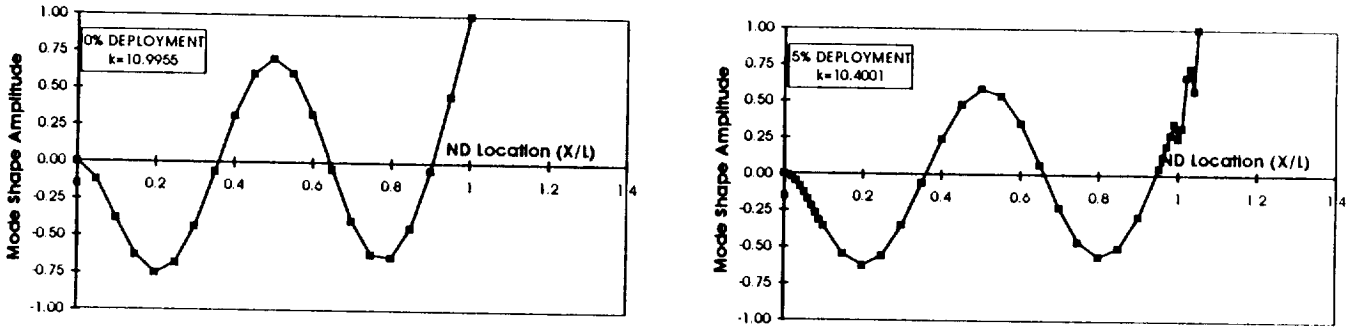

Figure 8: Mode 4 Shapes for 0% & 5% Deployment

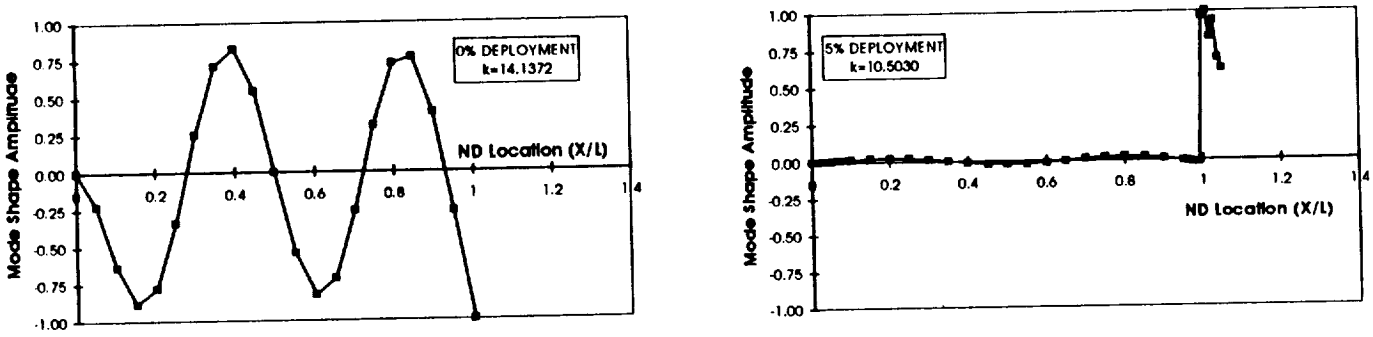

Figure 9: Mode 5 shapes for 0% & 5% Deployment

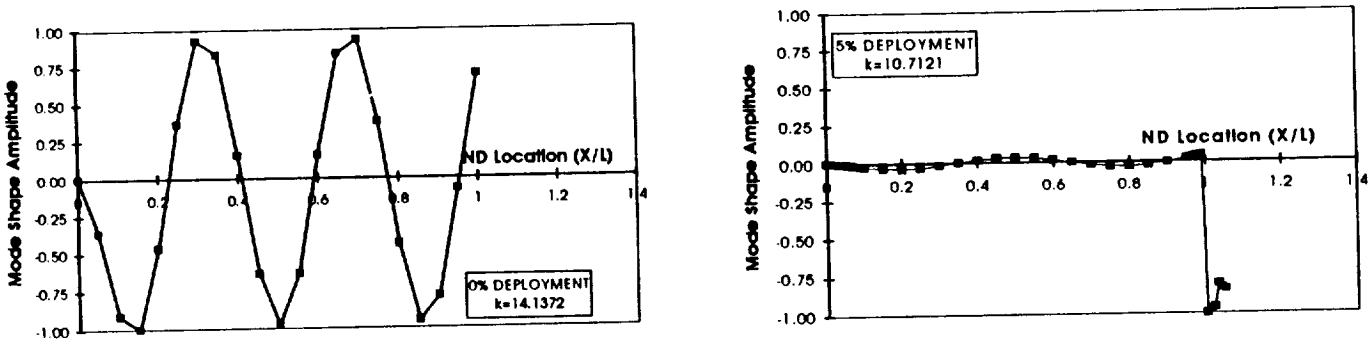

Figure 10: Mode 6 shapes for 0% & 5% Deployment

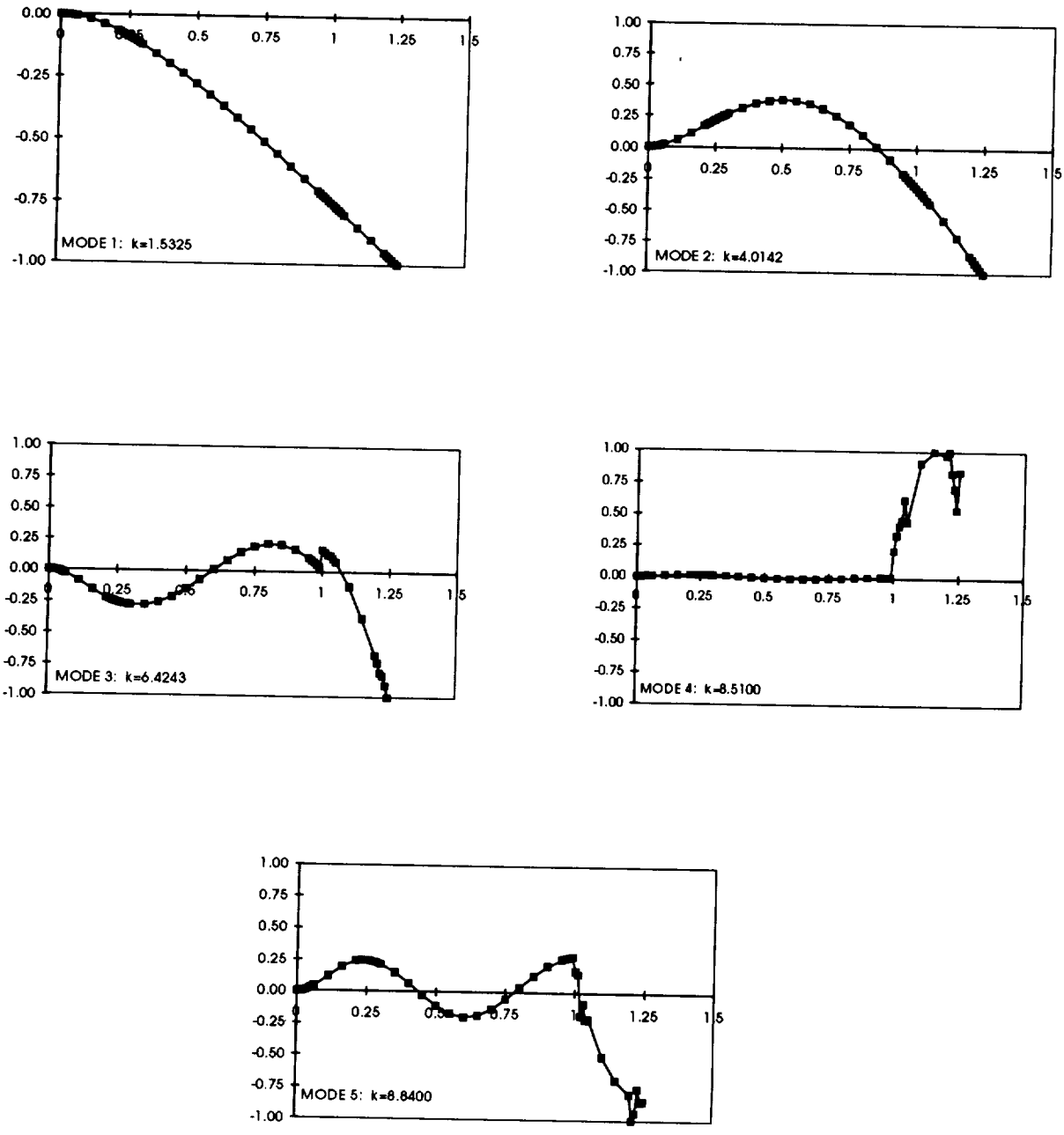

Figure 11: Mode Shapes at 25% Deployment

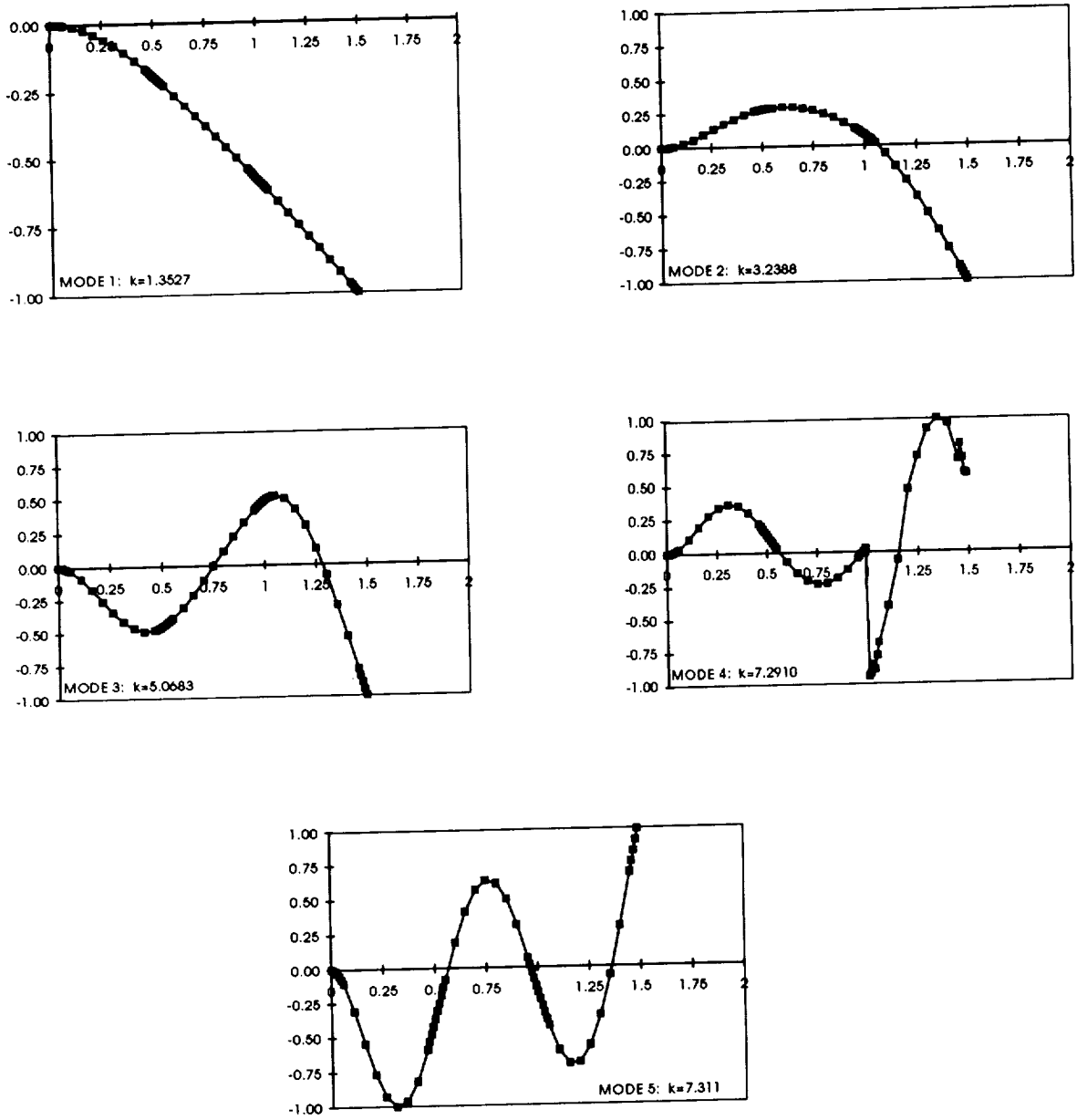

Figure 12: Mode Shapes at 50% Deployment

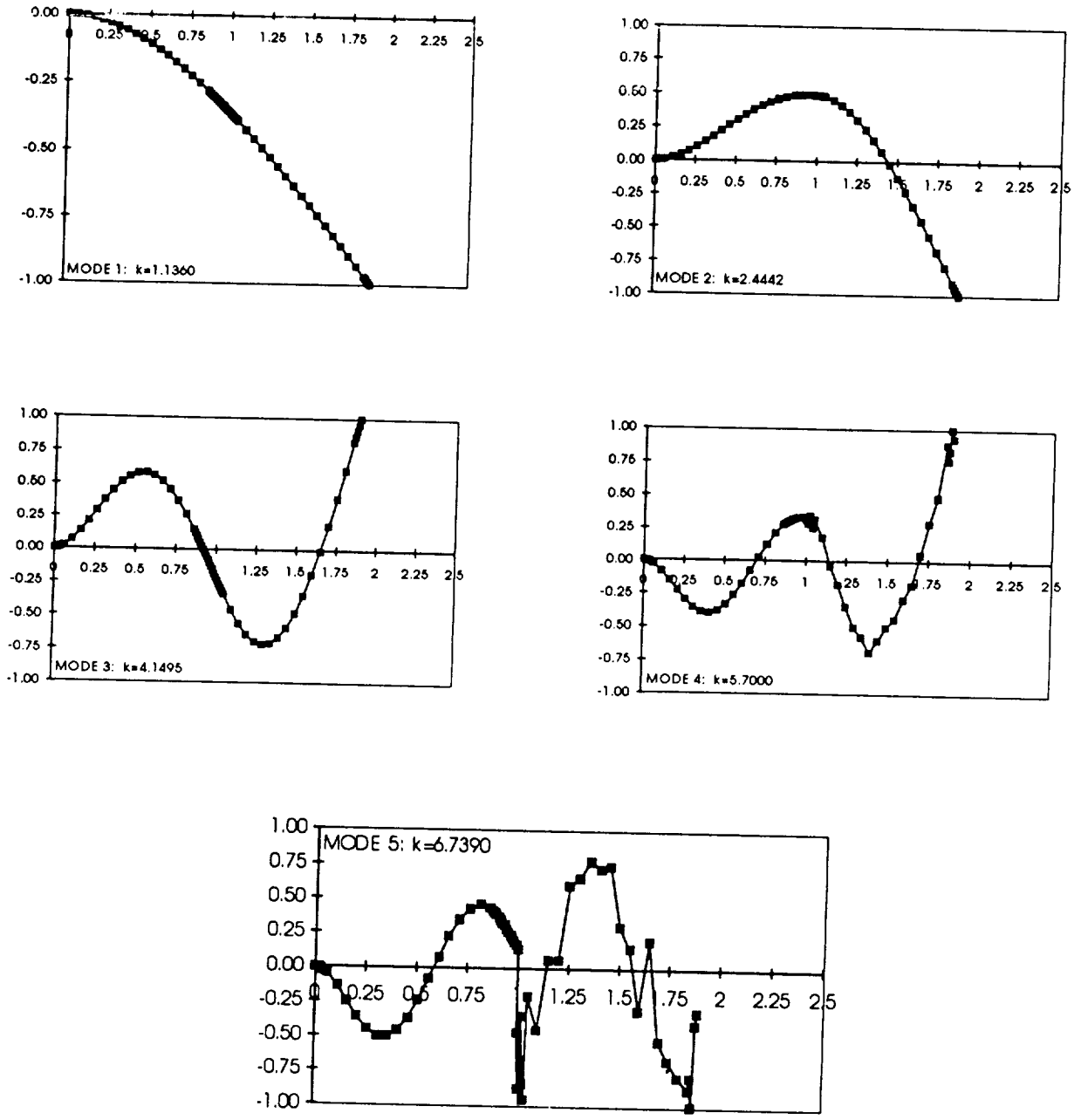

Figure 13: Mode Shapes at 90% Deployment

AEROELASTICITY APPLICATIONS